“Ponderosa Pilots”

SAE Aero Design West, Team #49
Northern Arizona University

Technical Design Report

Jacob Cong

Chris Galus

Alex Klausenstock

Nathan Valenzuela

2019-2020

Project Sponsor: W.L. Gore and Associates Inc.

Faculty Advisors: Dr. John Tester, Dr. David Trevas

STATEMENT OF COMPLIANCE

Certification of Qualification

Team Name	Ponderosa Pilots	Team Number	49
School	Northern Arizona University		
Faculty Advisor	Dr. John Tester		
Faculty Advisor's Email	John.Tester@nau.edu		

Statement of Compliance

As faculty Adviser:

JTT (Initial) I certify that the registered team members are enrolled in collegiate courses.

JTT (Initial) I certify that this team has designed and constructed the radio-controlled aircraft in the past nine (9) months with the intention to use this aircraft in the **2020** SAE Aero Design competition, without direct assistance from professional engineers, R/C model experts, and/or related professionals.

JTT (Initial) I certify that this year's Design Report has original content written by members of this year's team.

JTT (Initial) I certify that all reused content have been properly referenced and is in compliance with the University's plagiarism and reuse policies.

JTT (Initial) I certify that the team has used the Aero Design inspection checklist to inspect their aircraft before arrival at Technical Inspection and that the team will present this completed checklist, signed by the Faculty Advisor or Team Captain, to the inspectors before Technical Inspection begins.

Signature of Faculty Advisor — Date: 2/20/20

Signature of Team Captain — Date: 2.20.20

Table of Contents

1 Executive Summary

This report describes the procedure and outcome of the design process for the fixed wing aircraft built to compete in the 2020 Society of Automotive Engineers (SAE) Aero Design West competition. Included in this document are the preliminary design process, manufacturing techniques, physical and computational analysis of device performance, details about testing iteration, and optimization of the design. Physical testing of the aircraft provided proven results to match the outputs from programs such as Open Vehicle Sketch Pad (VSP), MATLAB and Microsoft Excel. Empirical testing data as well as the computational analysis have proven that the aircraft designed and built by the team is able to takeoff in the required distance and carry the necessary payload as per the 2020 rules document from SAE [1]. With a collection of flight test data along with a modular and easily repairable device, the team is confident that good flight scores and good overall performance at competition is possible. By attending and competing in this design competition, Northern Arizona University is represented among many other engineering colleges around the western United States and the team gains substantial experience in flight design, manufacturing methods, and general problem solving.

1.1 System Overview & Competition Projections/Conclusions

The design submitted by this team exploits the competition scoring equation by presenting a small plane with a high lift-to-span ratio. The small aircraft will include an aerodynamic cabin with a 10-inch cargo bay that encloses one soccer ball and 6.25 pounds of steel plate payload. Thrust provided by a single, 16x8 propeller will get the aircraft up to speed, allowing its small, 60-inch wings to generate enough lift to takeoff within the required 100-foot runway. Following the design phase of the aircraft, the team has performed numerous calculations, simulations, and prototype testing- all of which have led the team to predict flight scores of 14.14 points per round. Additionally, the team intends to earn at least 9 out of 10 of the payload prediction points.

2 Schedule Summary

As shown below in *Table 1*, the team created a schedule to outline specific due dates and working duration for each aspect of the project. A more comprehensive graphical representation can be found in *Appendix A*. Start dates in black text represent competition deliverables and blue text represents design class deliverables. Working dates that have passed are displayed in red text, effectively showing the current state of the project. At this point the team is on schedule and has completed full-scale prototyping to prove the success of concepts. This is in preparation for the final design submissions. All team members have taken part in each task, and all deliverables have been completed before specified end dates.

Table 1: Project Schedule

START DATE	END DATE	Acutal Due Date	DESCRIPTION	DURATION
9/29/19	10/18/19	11/5/19	Presentation 3	19
10/13/19	10/27/19	10/29/19	Website update	14
10/13/19	10/14/19	10/14/19	Register For Competition	1
10/13/19	11/10/19	11/12/19	Final Report	27
10/20/19	11/24/19	11/26/19	Final BOM and CAD	34
11/5/19	12/1/19	12/3/19	Protoype demo	26
11/10/19	12/1/19	12/3/19	Website check 2	21
11/10/19	12/8/19	12/10/19	Analytic Report Due	28
11/24/19	1/20/20	1/20/20	SAE Design Report	56
11/24/19	1/20/20	1/20/20	SAE 2D Drawings	56
11/24/19	1/20/20	1/20/20	SAE Tech Sheet	56
1/19/20	2/9/20	2/11/20	Hardware review	20
2/2/20	2/16/20	2/18/20	Website check 3	14
2/16/20	3/1/20	3/3/20	Midpoint pres/report	15
2/23/20	3/8/20	3/10/20	individual analysis 2	15
3/1/20	3/15/20	3/24/20	Final Product	14
3/1/20	3/22/20	3/24/20	Device summary	21
3/22/20	3/29/20	3/31/20	Draft of poster	7
4/3/20	4/5/20	4/5/20	Competition	2
3/22/20	4/5/20	4/7/20	Testing proof	13
3/29/20	4/12/20	4/14/20	Final Poster	13
3/29/20	4/12/20	4/14/20	Operation manual	13
4/5/20	4/19/20	4/21/20	Final Presentation	14
3/29/20	4/24/20	4/24/20	UGRADS	25
4/5/20	4/26/20	4/28/20	Final report and CAD	21
4/12/20	4/26/20	5/3/20	Final website	14

3 Table of References and Specifications

Table of Figures

Table of Tables

Table of Acronyms

CL:	Coefficient of lift for a wing
Cl:	Coefficient of lift for an airfoil
CDtot:	Coefficient of drag for a wing
Re:	Reynold's Number
AR:	Aspect Ratio

Works Cited

[1] Society of Automotive Engineers, "2020 SAE Aero Design Rules," [Online]. Available: http://www.saeaerodesign.com/cdsweb/gen/DocumentResources.aspx.

[2] "S1223 (5.64%) (S1223-il)," Airfoiltools.com, 2019.

[3] "NASA/LANGLEY LS(1)-0421," Airfoiltools.com, 2019.

[4] "NACA 0012 AIRFOILS (n0012-il)," Airfoiltools.com, 2019.

[5] J. D. Anderson, Fundamentals of aerodynamics, New York, NY: McGraw-Hill Education, 2017.

[6] D. Scholz, Aircraft Design, Berlin: Springer, 2012.

[7] "Propeller Static & Dynamic Thrust Calculation," Flite Test, [Online]. Available: https://www.flitetest.com/articles/propeller-static-dynamic-thrust-calculation. [Accessed 14 October 2019].

[8] "Aircraft Design High Lift Fzt.haw-hamburg.de.," [Online]. Available: https://www.fzt.haw-hamburg.de/pers/Scholz/HOOU/AircraftDesign_8_HighLift.pdf. [Accessed 209 December 2019].

[9] F. E. WEICK and C. J. WENZINGER, "The characteristics of a clark Y wing model equipped with several forms of low-drag fixed-slots," National Advisory Committee for Aeronautics, 1932.

[10] "Fort Worth Meacham International Airport, TX.," Weather Underground, [Online]. Available: https://www.wunderground.com/history/monthly/us/tx/fort-worth/KFTW/date/2018-4. [Accessed 13 December 2019].

[11] Recoskie, Steven & Lanteigne, Eric & Gueaieb and Wail, "A High-Fidelity Energy Efficient Path Planner for Unmanned Airships," 2017. [Online].

[12] "Aluminum Alloys - Mechanical Properties," Engineering ToolBox, 2008. [Online]. Available: https://www.engineeringtoolbox.com/properties-aluminum-pipe-d_1340.html. [Accessed 2019].

[13] M. Sadraey, "Chapter 9: Landing Gear Design,," in *Aircraft Design: A Systems Engineering Approach*, Wiley, 2012, pp. 479-544.

4 Design Process

4.1 Competitive Scoring and Strategy Analysis

The team began the design process by analyzing the scoring criteria outlined by the competition.

$$FS = Flight\ Score = 120 * \frac{2 * S + W_{steel}}{b\ + L_{cargo}} \quad [1]$$

$S = Number\ of\ Spherical\ Cargo\ Carried\ on\ a\ Flight$
$W_{steel} = Regular\ Boxed\ Cargo\ Weight\ (lbs)$
$b = Aircraft\ Wingspan\ (inches)$
$L_{cargo} = Length\ of\ Cargo\ Bay\ (inches)$

A score analysis Excel was created and design parameters were varied. From assessment, flight scoring was found to be driven primarily by generated lift divided by wingspan length. Additionally, payload cabin length plays an important role and should be kept as short as possible. As such, a short wingspan aircraft, carrying a single ball, with steel weights was the best design option. Considering these selections, the team recognized that the plane should be as light as possible, produce high lift, incur little drag, and be reliable.

4.2 Vehicle Configuration: Overall Design Layout and Size

The short wingspan and resultant reduced planform lifting area proposed a challenge of implementing a cabin design that could hold large spherical cargo. In an effort to maximize coefficient of lift while having a high height-to-chord ratio to accommodate the ball cargo, the team shaped the cabin and fuselage into a separate lifting body that will be referred to as “Ballfoil.” The Ballfoil assists in working toward the overall goal of attempting to increase lift per span by utilizing the cabin space as a lifting surface. In this way it does not waste scoring span without producing lift. One incidental benefit of the Ballfoil is that it acts as the mounting plate and lever arm for the empennage due to its length (52-inches). A short 60-inch wingspan, deep 18-inch chord, and a high-lift airfoil was chosen for the wing in an attempt to keep flight scores high. Additionally, to aid in the short takeoff distance requirement and increase total possible payload; leading edge slats and wing tip taper were employed. The landing gear configuration is taildragger.

This allows for reduced landing gear weight, default angle of attack, and an improved in-air center of gravity. In an effort to reduce unloaded weight and increase possible payload; low-density materials were studied and expanded polystyrene (EPS) foam was chosen to be the main constituent of the aircraft and is implemented in all lifting bodies.

4.3 Wing: Planform Design and Airfoil Selection

After studying multiple wing configurations, styles, advantages, and implementation, the team chose a small number of airfoils and configurations to study further. To achieve the greatest amount of lift-per-inch of wingspan, a tapered wing with leading-edge slats along the constant chord length section was fixed in a low mounting position. The leading-edge slats increase the velocity of the flow across the wing and tapering mitigates downwash effects. Airfoil type was studied by utilizing the online resource airfoiltools.com, which gives information on coefficient of lift, drag, and moment for various angles of attack at Reynolds Numbers (Re) [2]. The team searched for the best performing airfoil at the velocity and Re that it would be experiencing during the competition flights. In addition, a list was created by benchmarking the best industry short takeoff and landing (STOL) aircraft and the airfoils they utilized in practice. With these methods the team chose to manufacture the S1223 as the main lifting airfoil for prototype testing due to the large coefficient of lift (2.3) at an angle of attack of 16° near the operational velocity [2]. The aforementioned Ballfoil airfoil was difficult to choose due to the nature of the spherical cargo, and after many size tests a NASA/LANGLEY LS(1)-0421 was selected [3]. Notedly, it is estimated to produce 20% of the aircraft's lift. Finally, a variation of the NACA 0012 airfoil was chosen for the horizontal stabilizer, which will be used in its entirety as a control surface [4].

4.4 Drag Analysis (including 3D drag effects)

Induced drag is especially relevant to the design because Ballfoil is large, and its low aspect ratio (AR) make induced flow effects relatively large. These will be analyzed in depth in section 6.2.4. Study and analyses have shown that downwash effects make the lifting area near tips of the wings

less effective as induced angle of attack is then closer to zero. In response, the wing tips are tapered to limit such phenomenon. Additionally, the lift that is produced by the wing tips has a component tilted backward, which turns a component of the lift into induced drag. Alternatively, the team could have used an elliptical planform or wing twist to mitigate these negative effects, but for ease of manufacturing the team has refrained [5].

4.5 Stability and Control

Stability and control stem from a variety of factors; the most important of which are empennage and control surface sizing. The team sized the empennage according to the "Tail Volume Method" detailed in Scholz' *Aircraft Design* [6]. Because of constant changes in the design of the plane, the team input the Tail Volume equations into Solidworks so that each iteration of the design would automatically size the empennage for correct moment resistance. Control surfaces were sized using ratios provided by *Aircraft Design*. The sizing of these surfaces was put to the test in simulations (*see Section 6.2.2*), and prototype testing would eventually inform changes to control surface sizing (*see Section 7*).

4.6 Power Performance (Static and Dynamic Thrust)

The team borrowed a Turnigy static thrust test bed from NAU's Dr. Michael Shafer. It was calibrated using weights and used to test the static thrust of propellers with various diameters and pitches. During testing the team used the same battery, motor, competition specified power limiter, and controller to keep results consistent. After completing multiple rounds of testing, the data was recorded in units of kilograms. From these tests the following data presented in *Table 2* shows that statically the 16x8 propeller from Master Airscrew provided the greatest static thrust.

Table 2: Static Thrust Testing Results

				Wooden Test Apparatus	Turnigy Static Test Apparatus	Force
Propeller	Specs	Diameter (in)	Pitch (in)	(Kg)	(Kg)	N
A	18x8 Carbon Fiber	18	8	3.75	3.813	37.41
B	16x12	16	12	3.3	3.927	38.52
C	16x4	16	4	3.15	2.622	25.72
D	16x6	16	6	4.3	3.83	37.57
E	16x8	16	8	4.6	4.107	40.29
F	15x10	15	10	3.45	3.32	32.57
G	14x6	14	6	3.7	2.56	25.11
H	15x6	15	6	4.25	2.948	28.92

When choosing the propeller that would be used for our flight tests, these results had to be used to obtain dynamic thrust. Consultation with last year's team provided the Ponderosa Pilots with an equation that could be used to derive dynamic thrust from static results, provided rotations-per-minute of the motor being used could be found [7]. From these calculations it was found that propeller pitch was the greatest factor for increasing dynamic thrust. Post-testing, the team confirmed that 16x8 was the final selection.

4.7 Design Features and Details (Subassembly Sizing)

Sizing of the main wing and Ballfoil was discussed in *section 4.3* above. Leading edge slats were sized and placed pursuant to the guidelines given by NACA-TR-407 and based on the leading edge contour of the S1223 airfoil [8] [9]. The vertical and horizontal stabilizers were placed and sized based on distance from the main wings and chord length according to industry data from Scholz [6]. The location of the subassemblies and electronics as well as the placement of landing gear depended on situating the empty and loaded CG toward the center of lift and within the wheelbase.

4.8 Interfaces and Attachments

Main components of the aircraft mount to a 1-inch, aluminum, hollow, square tube of 1/20$_{th}$-inch thickness. The motor is attached to the main bar by a custom designed mount and five steel mounting bolts. All of the main electronic control devices are situated in a custom mount, fitted to the main bar with the battery segregated in a compartment below. By utilizing hollow aluminum

tubing passing through the side of the EPS Ballfoil and main bar, a rigid and robust body is created. The main bar also serves as the conduit for internal electronic wiring. Both landing gears was connected to the main bar with bolts. To affix objects to the EPS that cannot be attached to the main bar, epoxy was used to create a strong adhesive bond. It is also used to compile sections of the wings, ballfoil, and other control surfaces. Additionally, epoxy was used on each of the mounting rods for the leading-edge slats, as well as to attach all of the control surface horns. The servos actuating control surfaces were custom-fit into EPS and mounted using silicone. All threaded connections feature a positive locking nut and/or supplementary thread-locking adhesive.

5 Loads and Environmental Assumptions

Before analysis could be conducted, testing loads, environments, and other assumptions had to be considered. The following sections will detail how those items were derived and under what conditions the team's analysis was conducted. Inviscid and incompressible flow were assumed for calculations.

5.1 Design Load Derivations (Accelerations, Landing Shock, etc.)

When designing the landing gear, the team calculated expected landing forces and determined that allowing a higher impact distance was the best course of action. This would allow minimal material to be used while providing sufficient structural support. The main (front) gear was constructed from a single aluminum bar and functions as a spring in tandem with an additional spring in tension between the wheels to prevent deformation of the gear. The secondary (rear) steering gear design features a smaller aluminum bar bent to shape.

Table 3: Impact Force Calculation

Impact Force			
Weight	w	18	lbs
Mass	m	8.1647	kg
Distance	h	1	ft
		0.3048	m
Gravity	g	9.81	m/s^2
Delta Time	t	0.2493	s
Delta Velocity	V	2.4454	m/s
Impact Distance	ΔD	0.05	m
Impact Force	F	488.26	N

This landing gear setup provides the damping needed to support the 488.26 Newton landing force from a 1-foot drop, as calculated above in *Table 3*.

5.2 Environmental Considerations

Before simulations could be run, the team needed to decide appropriate airflows for ideal flight, windy flight, and flight with gust-winds. To do this, weather data from Ft. Worth, Texas was acquired from Weather Underground's archive [10]. This data was scaled back using wind speed graphs compiled by Recoskie and Lanteigne [11].

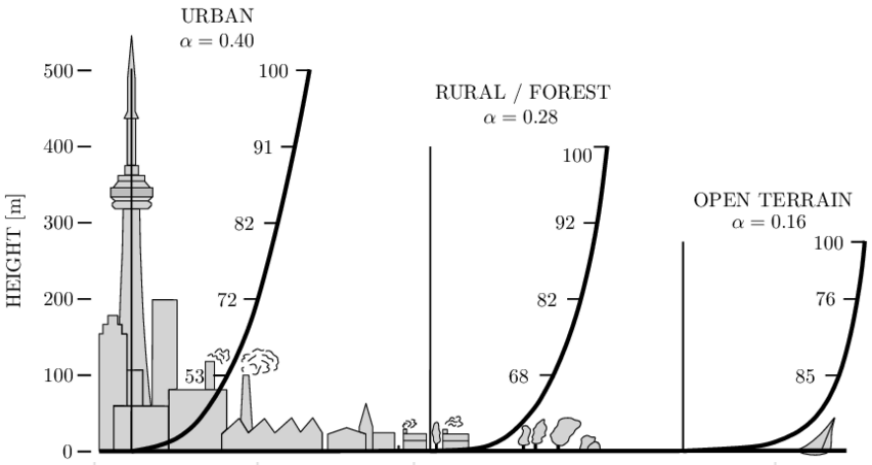

	Altitude (ft)	Wind Speed (mph)
Avg. Wind	25	5.68
Gust Wind	25	14.71

Figure 1: Wind Speed Data

These values could be added to flow vectors in the simulations shown in *Section 6.2.2*. A critical assumption made was that the "worst-case" wind vector would occur when gust-wind hit the plane directly from the side.

6 Analysis

6.1 Analysis Techniques: Analytical Tools (CAD, FEM, CFD, etc.)

Open VSP was used to model inviscid, incompressible, 3-dimensional lift characteristics of our proposed design and planform. The wing, ballfoil and horizontal stabilizer were modeled in this program.

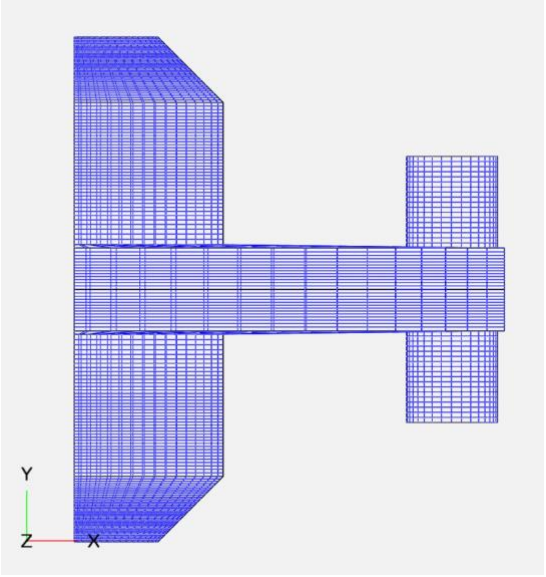

Figure 2: Open VSP Model

This program utilizes Prandtl's lifting line method and the vortex sheet method. It also effectively found CL and CDtot for our wing planforms which was later used in a novel iterative Excel lift calculator to determine performance. Using Open VSP and the iterative Excel lift calculator, span and chord were iterated until optimal lift was yielded (*See section 6.2.4 for further information on Iterative Excel Lift Calculator*). Solidworks was also used as a CAD and CFD tool to further evaluate control surface performance.

6.2 Performance Analysis

6.2.1 Runway/Launch/Landing Performance

The landing gear configuration of the craft is taildragger. With a base angle of attack of 16 degrees, the resting height of the elevator is 3.75 inches from the ground. This default angle of attack assists the aircraft to liftoff within the specified 100-foot runway. The impact-damping suspension within the design allows for smoother landings and lessened impact forces.

6.2.2 Flight and Maneuver Performance

To test flight and maneuver performance, Solidworks flow simulations were conducted. These simulations would reveal whether or not the plane's control surfaces were properly sized. A plane velocity of 20 mph was assumed, and the gust wind from *Section 5.2* was added to the flow. A control test revealed that the plane needed to resist the following torques:

GG Torque (X) 1	0.254429 N*m
GG Torque (Y) 1	1.43936 N*m
GG Torque (Z) 1	1.30626 N*m

Figure 3: Torques Created by Wind

Once these values were generated, the aircraft was again put in the path of a flow vector, this time with angled control surfaces. By angling the control surfaces, the team was able to reduce torques around the X and Z axes to zero. Based on previous flight experience, torques around the Y axis (Yaw) are of no concern. The plane will adjust its own trajectory to reduce that torque. With this in mind, the team can verify that the aircraft's control surfaces are adequately sized to resist torques imposed by wind gusts.

6.2.3 Shading/Downwash

Downwash was considered in two components of our design process. During the preliminary stage, a graph of maximum CL for a NACA wing versus aspect ratio was studied [5].

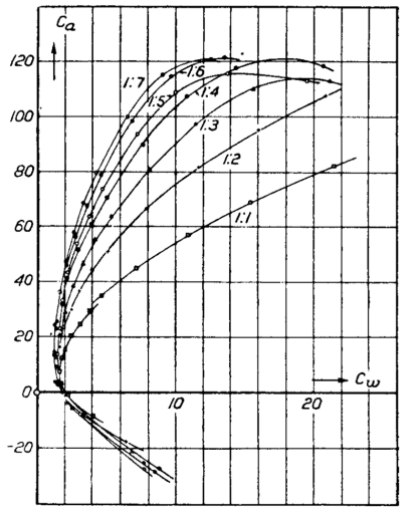

Figure 4: Varying CL vs. CDtot for Varying Aspect Ratio

In this nomenclature, *Ca* = CL and *C*w = CDtot. Also, the CL and CDtot are 100 times the actual values [5]. The figure above shows a trend that the CL decreases exponentially after AR drops below approximately 3. These losses are attributed to induced angle of attack caused by downwash flow. Therefore, it was assumed that an aspect ratio greater than 2.5 should be maintained. Later, when 3D effects of downwash were simulated with Open VSP, the trend in the figure above held true for wings with no tapering. Since CL is almost directly proportional to angle of attack, we can use it as a proxy for induced angle of attack caused by the vector sum of downwash and incoming flow. Below we can see a plot of CL decreasing on the main wings near the tips where downwash is more prevalent.

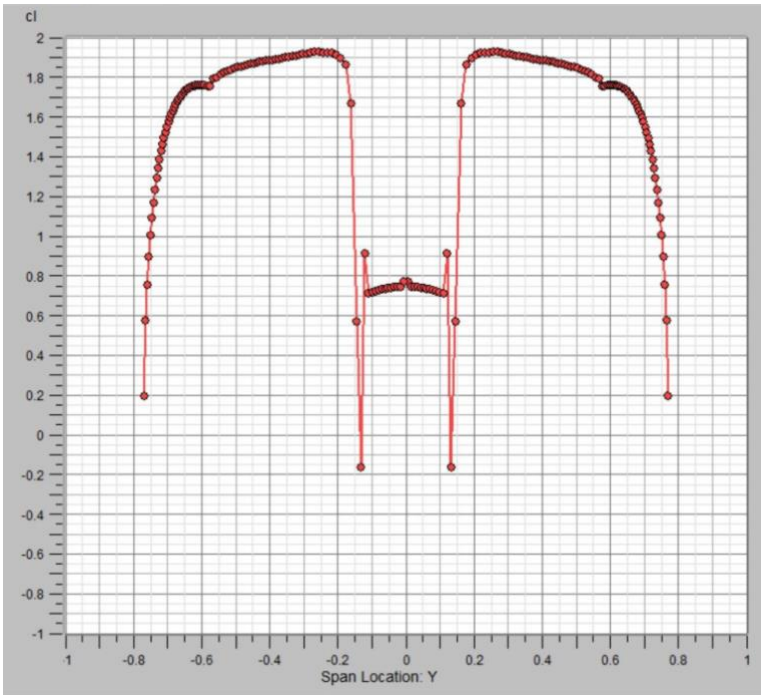

Figure 5: Span-Wise CL

6.2.4 Lifting Performance, Payload Prediction, and Margin

The lifting performance has to consider a large number of variables, including distance to takeoff, total mass, dynamic thrust, 3D wing performance, and more. Eventually, other design and manufacturing decisions constrained a number of these variables, leaving only wingspan and chord to vary in order to achieve an optimal scoring and lifting wing. Changing these two variables have

less than obvious effects due to 3D flow phenomena related to aspect ratio and downwash. Lift, velocity, planform area, and CL are interrelated. Thus, an iterative method was set up to calculate lift and scoring potential for a number of different spans with different chord lengths, each at regular intervals. From this score and lift data we can effectively interpolate what the optimal planform shape would be for the given constraints. The lift calculation itself was based on an iterative model which determined the takeoff velocity at the end of the runway. From this velocity we can determine lift for a given planform, which has its own corresponding CL, that we have determined does not vary appreciably over velocity. This lift-minus-empty-mass is our predicted payload. At this point in time there is no margin; however, it is anticipated that a significant margin will be added from increasing air density relative to our test site.

One notable simplification made to the calculations was the assumption that CL did not vary with velocity as was inferred by airfoil data charts [4]. This simplification was found by looking at a simulation plot between Mach and CL.

Table 4: Excel Lift Calculator Example Iteration

Propeller Properties	
Prop	Tested
Pitch	8
Diam	16
RPM	7484

Airfoil Properties	
Airfoil	S1223
Planform Area (m^2)	1.09
CD	0.320
CL	1.445

Misc Parameters	
Weight (lbs)	17.00
Mass	7.71
Air Density	0.95
Time Interval (s)	0.05

Planform Area Calculator			
Part	Span (m)	Chord (m)	Total
Main Foils	0.635	0.4572	0.581
Ball Foil	0.127	1.1303	0.287
Empennage HS	0.2794	0.4064	0.227
		Total	1.095

Time (s)	Distance (dx) (m)	Velocity (m/s)	Thrust (N)	Drag (N)	Acceleration (m/s)	Lift (N)	Lift (Lb)	Score @ this velocity		Score per run
0	0.00	0.00	37.4	0.0	4.85	0.0	0.0	-17.9		12.0
0.05	0.00	0.24	37.1	0.0	4.81	0.0	0.0	-17.1		
0.10	0.01	0.48	36.7	0.0	4.76	0.2	0.0	-17.1		
0.15	0.04	0.72	36.4	0.1	4.70	0.4	0.1	-17.0		
0.20	0.07	0.96	36.0	0.2	4.65	0.7	0.2	-16.9		
0.25	0.12	1.19	35.7	0.2	4.60	1.1	0.2	-16.7		
3.70	22.86	9.87	22.9	16.2	0.86	73.2	16.4	11.0		
3.75	23.35	9.91	22.8	16.3	0.84	73.8	16.6	11.3		
3.80	23.85	9.95	22.7	16.5	0.81	74.4	16.7	11.5		
3.85	24.35	9.99	22.7	16.6	0.78	75.0	16.9	11.8		
3.90	24.85	10.03	22.6	16.7	0.76	75.6	17.0	12.0		
3.95	25.35	10.07	22.6	16.9	0.74	76.2	17.1	12.2	past 85 ft	
4.00	25.85	10.11	22.5	17.0	0.71	76.7	17.3	12.4	past 85 ft	
4.05	26.36	10.14	22.5	17.1	0.69	77.3	17.4	12.6	past 85 ft	

The Payload Prediction Curve was derived by interpolating calculated lift at sea level and 7000 ft elevation. This was achieved by simply changing the air density to that of sea level in our excel calculator.

6.3 Structural Analysis

A key analysis aspect separate from the aerodynamics of the design is its structural soundness. The design presented by the team is supported by an all-aluminum frame, balanced upon a taildragger-style landing gear. The following sections will examine the loads and stresses on the frame. For an analysis on landing gear stresses, refer back to *Section 5.1*.

6.3.1 Mass Properties & Balance

Before any load analyses could be conducted, the team first needed to evaluate the aircraft's center of mass. Although computer tools such as Solidworks had tools for finding center of mass, the team decided that the most accurate way to assess center of mass would be to measure it on a full-scale prototype. After constructing a flight-successful prototype, the team used a balancing beam to find the plane's empty and loaded centers of mass. These are pictured in relation to the estimated center of lift in the figure below.

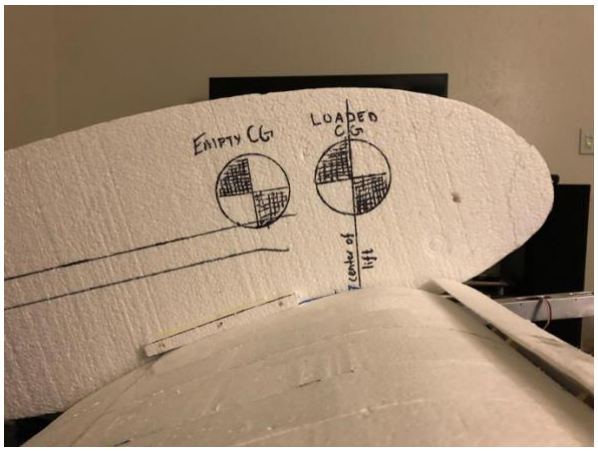

Figure 6: Empty and Loaded Centers of Gravity Pictured on "Ballfoil" Beside Center of Lift

The team believes that having a center of gravity in line with the center of lift will be the most ideal. This way, the in-flight moment equation is nearly balanced and the elevator will have to do limited work to keep the plane stable. The team's plane has an empty CG that is currently 4 inches behind the estimated center of lift, but by testing different payload positions with prototypes, the team was able to move the weighted CG in line with the center of lift. The calculations conducted

below keep the CG 1.5 inches behind the center of lift in an attempt to conduct a conservative, worst-case scenario.

6.3.2 Applied Loads and Critical Margins

As mentioned previously, the aircraft is supported by an aluminum frame. The two main frame components are the "Main Beam" and the "Wing Spar." The Main Beam is a hollow, square tube (I= 0.019). The Wing Spar is a smaller, hollow, square tube (I = 0.015). By treating these two members as straight beams, the team could calculate bending moments through the beams due to forces such as aircraft weight, wing lift force, empennage lift force, and ground reactions (from landing gear). Analysis was simplified by treating all forces as point loads. The layout for these calculations can be seen in *Appendix A1*. These calculations revealed maximum bending stresses of 741 psi and 2200 psi in the Main Beam and Wing Spar, respectively. Compared to aluminum's average yield strength of 40,000 psi, the structure is safe with a minimum factor of safety of 18 [12].

Table 5: Bending Stress Critical Margins Table

	$\sigma_{Experienced}$ (psi)	σ_{Yield} (psi)	Critical Margin (FOS)
Main Beam	741	40000	54
Wing Spar	2200	40000	18

6.4 Assembly and Subassembly, Test and Integration

The first testing conducted by the team was static propeller thrust, which included two iterations. See *Section 4.6 Power Performance* for details on static propeller thrust test. When assembly testing began, the original form of the craft featured zero angle of attack and a tricycle landing gear configuration. Additionally, the front landing gear design was bulky and ineffective, the tires were heavy rubber, and the elevator was undersized. See *Figure 9* for Pine Patrol One MK1.

Figure 7: Pine Patrol One MK1

The plane showed no sign of producing sufficient lift, and the next iteration included an angle of attack, along with lighter foam tires, a lighter and more simple front landing gear, and a larger elevator. This design proved successful at lifting off with additional weight in a simple, indoor, straight line test.

Figure 8: Pine Patrol One MK2

With snow on the ground, the team continued with indoor testing and the third iteration of the assembly now included leading edge slats and a housing unit for the LiPo battery along with a battery capacity reduction from 5000mAh to 3000mAh. With the installation of leading-edge slats, the prototype was able to lift approximately an additional 1.5 lbs. and, at dry weight, take off at the 30-foot mark. The final test of that prototype was conducted outdoors at the Flagstaff Flyers airfield. The craft became airborne and gained approximately 40 feet of elevation but failed to produce sufficient lift through the first turn. This caused the plane to slowly lose altitude before

crashing and ending the test session. The team attributes this failure to poor placement of the center of gravity in relation to the center of lift along with wind.

Figure 9: Pine Patrol One Mk4

To correct the in-flight center of gravity issues, the configuration was modified to taildragger. Additionally, the final iteration of prototype design featured a new main spar that extended back to the tail wheel and a new wing spar that was lighter. Taper was added to the tips of the wings and Ballfoil was increased 4 inches in chord. All electronics were compiled into a single mount at the front of the main beam. Finally, the horizonal stabilizer and elevator were combined into a single unit.

7 Manufacturing

The team found themselves with a calculation-proven and prototype-tested design. The following section will detail the manufacturing process, both for the prototypes and for the final design.

Discussion

A materials analysis led to the team's decision to craft their aircraft's aerodynamic surfaces from foam. EPS foam is easily accessible and has an incredibly low density of 15-50 kg/m^3. Because of EPS' tendency to fracture, all of the plane's foam surfaces are supported by a lightweight aluminum frame. All other aircraft components are fabricated with PLA plastic. All members are held together with adhesive or aluminum bolts.

Prototype

Construction of the aluminum frame and landing gear components was simple, fortunately. Most members of the team had been trained in aluminum fabrication at the University's machine shop, and the team had access to the required equipment (drill presses, band saws, end mills, lathes) in their or the University's possession. Members of the plane's frame were cut to size using a horizontal band saw, and aluminum flat beams were bent to shape using vices and mechanical advantage. These aluminum components had all mounting holes drilled with a drill press.

The EPS foam aerodynamic surfaces took more time to construct. The most effective and easiest way to shape EPS foam is with a hot-wire cutter. Because the team did not have access to a professional grade hot-wire cutter, one was constructed by the team. The hot wire cutter features a tensioned, nichrome wire, through which an electrical current is run from an off-the-shelf power supply. By manipulating the voltage and amperage through the wire, the team could heat the wire to the necessary temperature to melt foam. Other parts, such as the motor mount and the battery compartment were modelled in Solidworks and submitted to the University's "Maker Lab" for 3D printing.

Figure 10: Homemade Hot-Wire Cutter in Use

Finally, all components were assembled. Members of the aluminum frame were fastened with lightweight aluminum bolts. The nuts used with these bolts were all either positive locking or coated in thread-locking adhesive to prevent slipping due to vibration. Foam connections were made with adhesives. After finding that many glues melted the EPS, the team discovered that epoxy successfully held foam members together.

Future Work: Final Product

The team's final product will be manufactured using similar methods to the ones for the prototype described above. Some manufacturing processes the team hopes to implement on the final product include welded joints in the frame and landing gear, smoother hot-wire foam cutting, and magnetically sealed cargo bay doors.

8 Conclusion

The NAU Ponderosa Pilots' design process for the SAE Aero 2020 competition began by manipulating the competition scoring equation in respect to wingspan, cabin length, ball capacity, and plate weight capacity. Through these considerations, the final design resulted in a small plane with a high lift-to-span ratio. The small aircraft includes an aerodynamic cabin with a 10-inch cargo bay that encloses one soccer ball and 6.25 pounds of additional weighted payload. Thrust is provided by a single 16x8 propeller that will bring the aircraft to sufficient speed. The airfoil selected for the main wings is the S1223 and spans 50 inches of the total 60-inch wingspan, with an 18-inch chord. Leading edge slats and wing tip taper have been implemented to assist the aircraft in generating sufficient lift within the required 100-foot runway. The landing gear setup will also assist with the short takeoff distance as it is a taildragger setup with a base angle of attack of 16 degrees. Calculations, simulations, and prototype testing have helped to validate this design. The team's primary focuses include manufacturability, dynamic reliability, and scoring potential. Through iterative design and testing, the competition and team's goals have been successfully achieved along with a deeper understanding of aircraft design.

Appendix A – Supporting Documentation and Backup Calculation

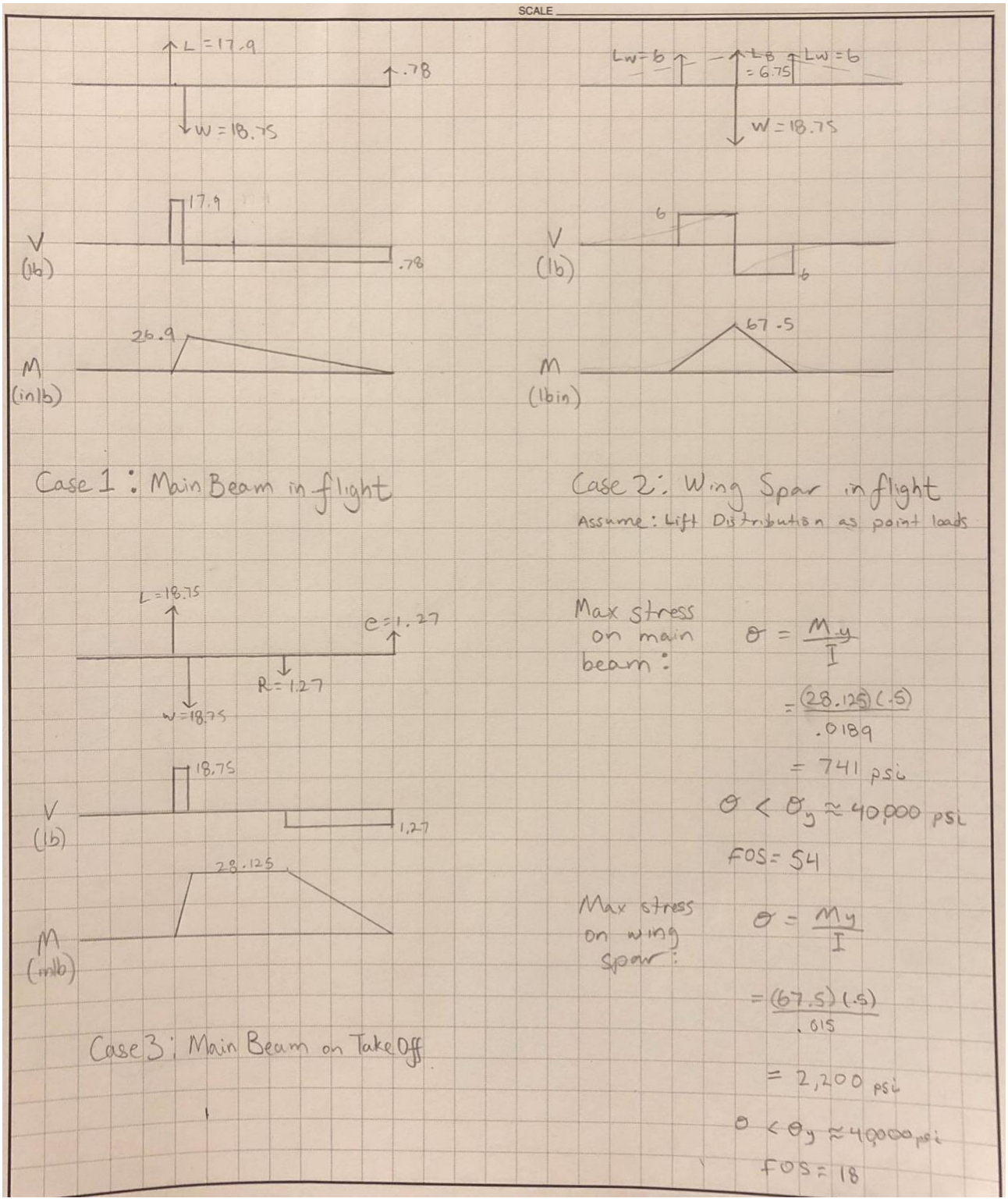

Figure 11-A: Structural Analysis

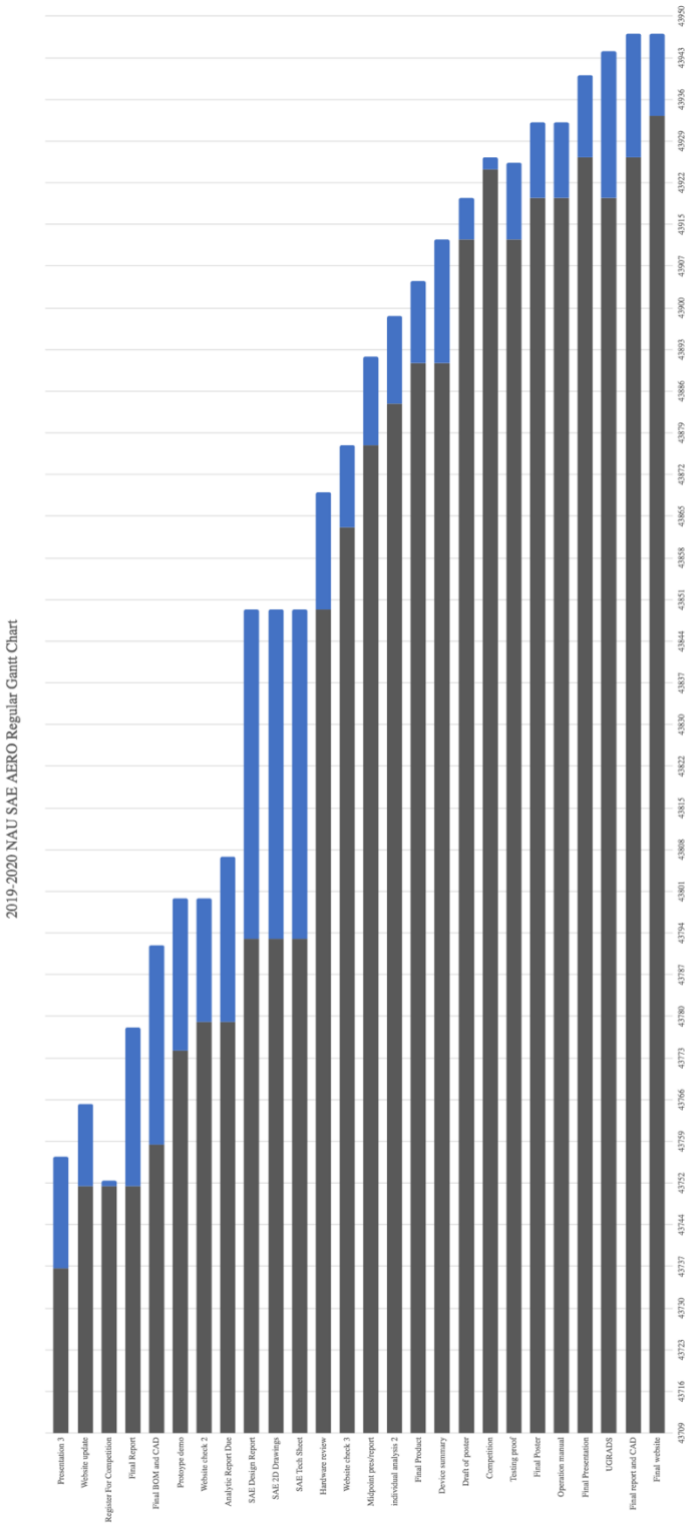

Figure 12-A: Team Gantt Chart

Appendix B – Technical Data Sheet

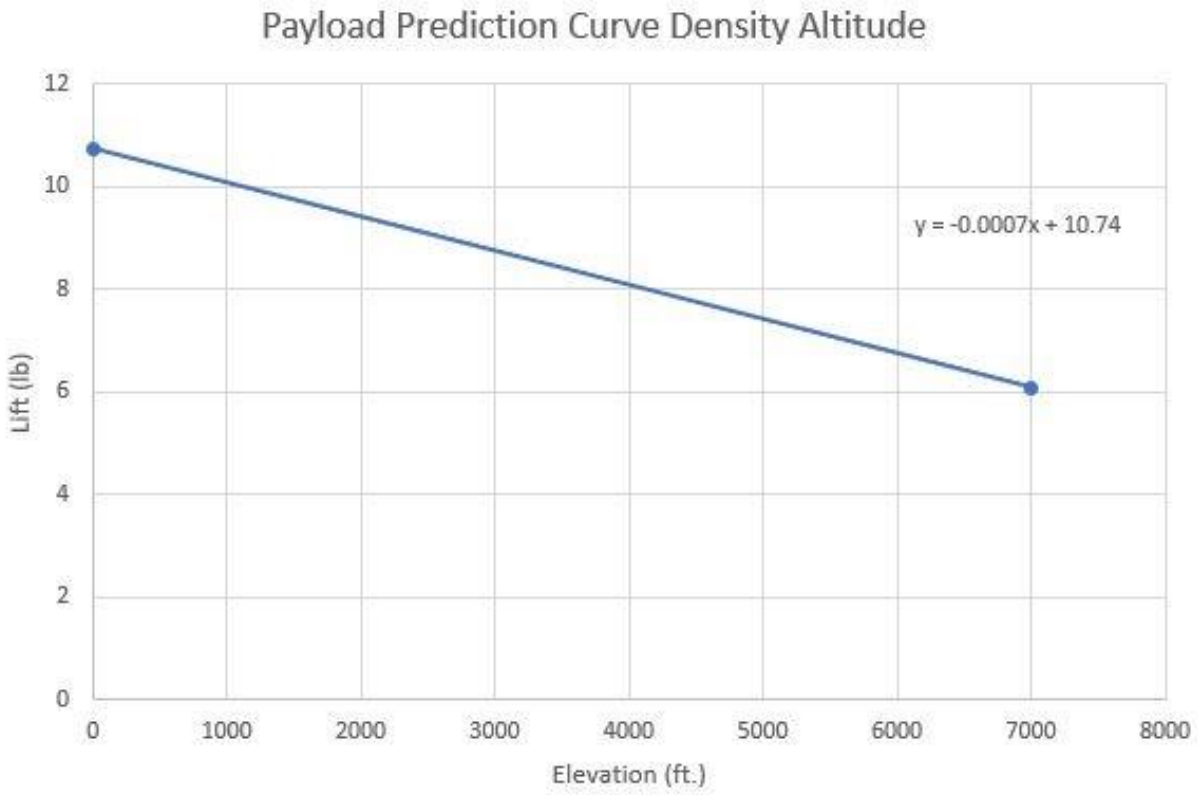

Figure 13-B: Payload Prediction Curve by Altitude Density (*See end of section 6.2.4 for Derivation of curve*)

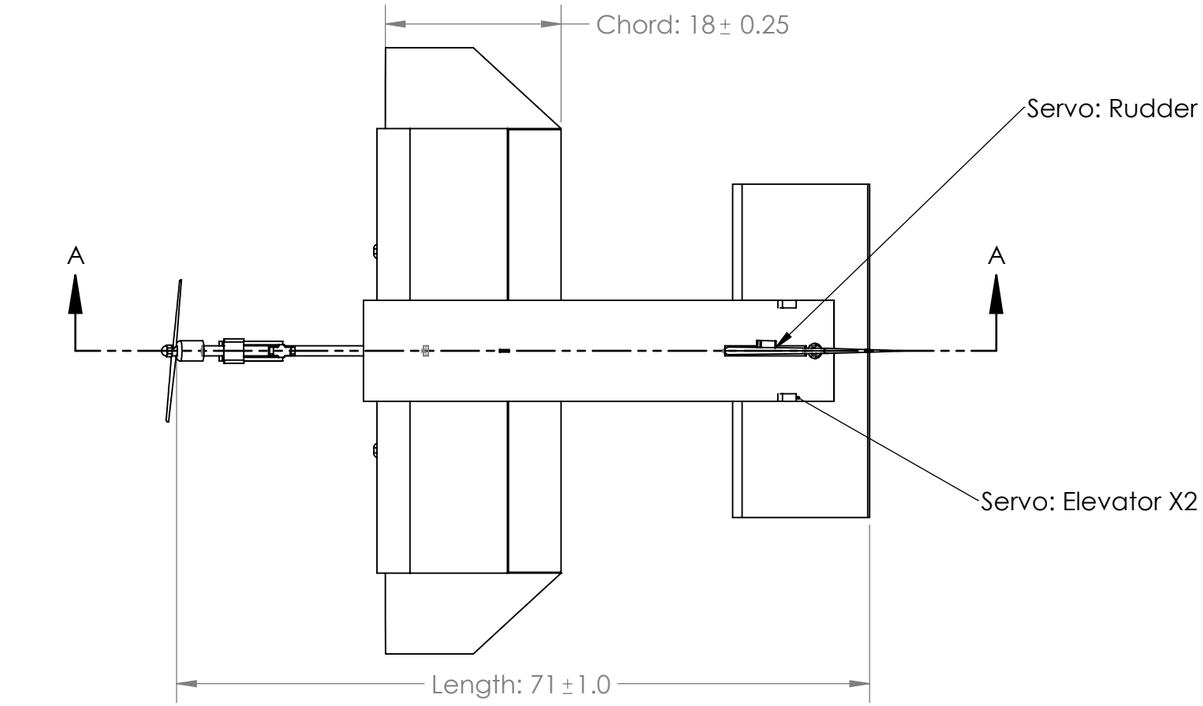

Wingspan (in)	60
Empty Weight (lbs)	9.05
Battery Capacity (mAh)	3000
Motor Spec	Neumotors 4625
Motor KV	540
Propeller Manufacturer	Master Airscrew
Propeller Diameter (in)	16
Propeller Pitch (in)	8
Servor Manufacturer	HiTEC
Servo Model #	HS-5625MG
Servo Torque (oz-in)	110

Item	Location from Datum (in)	Weight (lbs)	Resultant Moment (in-lbs)
Motor	4.0	0.81	3.24
Battery	10.0	1.08	10.8
Electronics Bay (ESC, Limiter)	10.0	0.53	5.3
Payload	26.0	7.15	185.9

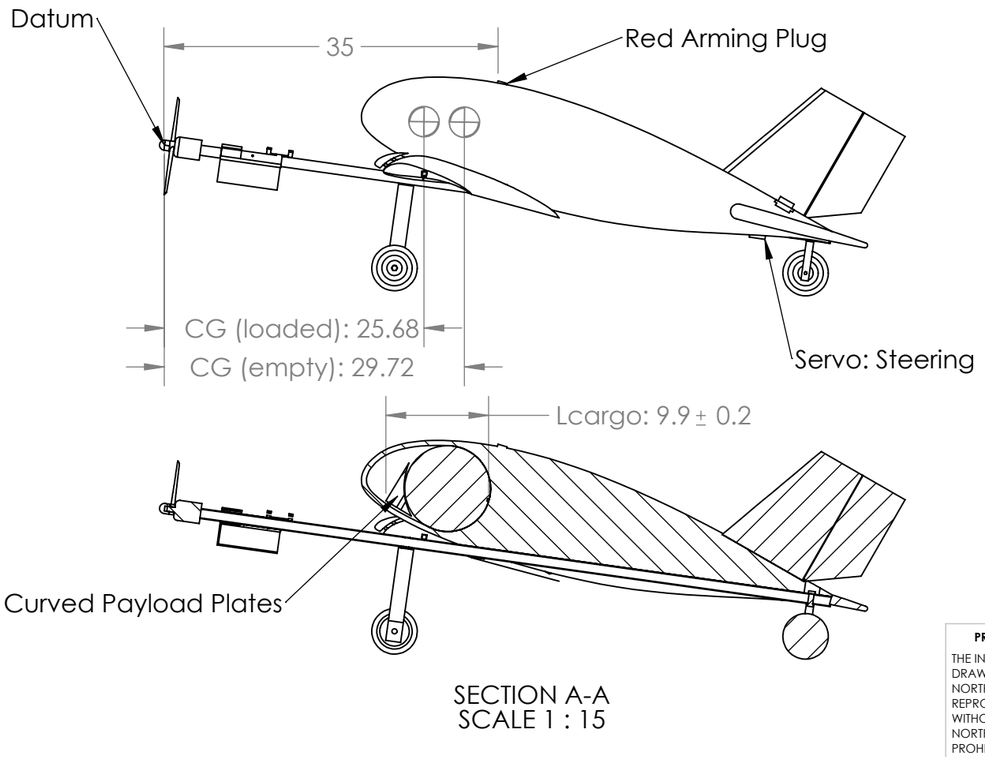

SECTION A-A
SCALE 1 : 15

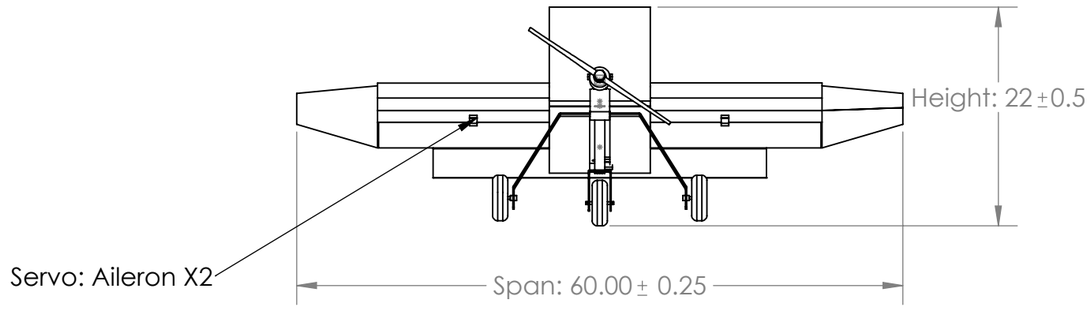

		UNLESS OTHERWISE SPECIFIED:		NAME	DATE
		DIMENSIONS ARE IN INCHES TOLERANCES: FRACTIONAL ± ANGULAR: MACH ± BEND ± TWO PLACE DECIMAL ± THREE PLACE DECIMAL ±	DRAWN		
			CHECKED		
			ENG APPR.		
			MFG APPR.		
		INTERPRET GEOMETRIC TOLERANCING PER:	Q.A.		
		MATERIAL	COMMENTS:		
NEXT ASSY	USED ON	FINISH			
APPLICATION		DO NOT SCALE DRAWING			

TITLE:
Ponderosa Pilots, Team #49
Northern Arizona University

SIZE	DWG. NO.	REV
B	2D Drawing	
SCALE1:15	WEIGHT:	SHEET 1 OF 1